PACS numbers: 42.62.Be, 42.62.If, 42.65.Re,
63.20.kd, **63.20.–e**, 78.47.J–, 78.47.jg
DOI: 10.3367/UFNe.0184.201406j.0672

Femtosecond spectroscopy of promising materials

S V Chekalin

1. Introduction

One of the most powerful tools for studying the dynamics and structure of various materials is nondestructive optical methods preserving all the functional properties of the samples in the performance of the exploration. Obviously, the properties of promising (next-generation) nanostructured materials are mainly determined by the spatial distribution of structural components, their mutual packing, and interaction. In turn, information about this can be obtained by studying the relaxation properties of matter. The nanometer sizes of subunits assume that the minimal relaxation times of excitations lie in the femtosecond range. Therefore, femtosecond spectroscopy can be applied for the study and certification of such materials. This was demonstrated in experiments on the ultrafast spectroscopy of photoinduced processes in fullerene–metal nanostructures of various types [1, 2], where a strong dependence of the relaxation observed was found on both the relationship between the quantities of metal and fullerenes and their mutual packing in samples.

Nearly the last 40 years of the 45-year history of the Institute of Spectroscopy, RAS (ISAN in *Russ. abbr.*) are concerned with ultrafast spectroscopy based on ultrashort laser pulses (USPs) [1]. Applications of USPs for scientific studies were initiated in 1973 with the advent of picosecond lasers (see monograph and theses [3] and references cited therein). At the same time, the generation mechanism of femtosecond pulses upon radiation self-focusing in an active element was disclosed in paper [4]. This mechanism is used in third-generation solid-state lasers [5] which have become the most popular. The first femtosecond dye laser in the USSR was launched at ISAN in 1979 [6]. However, a few years was required to develop the equipment for the first experimental study of the ultrafast dynamics with femtosecond time resolution [7]. In the early 2004, modern femtosecond equipment, based on third-generation lasers and developed at ISAN with the support of RAS and other institutions, was combined in one unique spectrometric facility at the Center of Collective Use (CCU) [1]. This allowed us to begin collaborative experiments with many Russian institutes, the number of them increasing continuously along with expanding experimental feasibilities of the facility.

S V Chekalin Institute of Spectroscopy, RAS,
Troitsk, Moscow, Russian Federation
E-mail: chekalin@isan.troitsk.ru

Uspekhi Fizicheskikh Nauk **184** (6) 672–680 (2014)
DOI: 10.3367/UFNr.0184.201406j.0672
Translated by M Sapozhnikov; edited by A Radzig

2. Femtosecond laser complex at the Center of Collective Use at the Institute of Spectroscopy, RAS

The Optical Spectral Studies laser facility at ISAN's CCU is described in detail in Ref. [1], and therefore we mention here only the expansion of its capacities for the last eight years:

(i) The output energy of a 800-nm laser pulse was increased to 4 mJ, and the pulse duration was shortened to 30 fs.

(ii) A terahertz channel was put in operation (see Section 4.2).

(iii) A pump–probe scheme based on a photoionization time-of-flight mass spectrometer equipped with a pulsed supersonic nozzle for studying the cluster dynamics was triggered (see Section 3.1.3).

(iv) Single-channel detection systems are being developed for the visible and IR ranges with a sensitivity up to 10^{-5}.

(v) Nanolocalized electron, ion, and X-ray sources based on microcapillaries were developed, and they can be positioned in space with a nanometer accuracy (see Sections 3.3 and 4.1).

3. Experiments on the equipment from the Center of Collective Use

In major experiments both under way and planned for the nearest future, two main lines of inquiry can be distinguished. The first concerns the femtosecond dynamics of various objects and next-generation materials; this study is performed by the pump–probe method. The equipment at CCU makes it possible to run such experiments using ultrashort UV, visible, and IR pulses in the region from 200 to 10,000 nm, terahertz (0.5–10 THz) pulses, nanolocalized electron and ion bunches, and soft X-ray pulses. The second direction is related to investigations that can considerably expand the capacity of the laser facility at CCU. They include the generation of ultrashort electron, ion, and X-ray beams, the efficient transformation of radiation to the terahertz range, the diffraction division of pulses, the search for optimal regimes of radiation conversion to supercontinuum, and the generation of 'light bullets'. Currently, extensive studies are in progress on the creation of a four-dimensional (4D) microscope.

3.1 Study of the femtosecond dynamics in free molecules and molecular complexes

3.1.1 Decay dynamics upon selective excitation of molecules at the fundamental vibrational frequencies of basic molecular bonds by femtosecond IR pulses in a gas phase. The excitation of one of the fundamental molecular vibrations for a time shorter than the characteristic time of the intramolecular vibrational energy redistribution (IVR) makes possible the initiation of bond- or group-of-bonds-selective photochemical reactions. In our previous experiments [8], we failed to perform the selective multiphoton excitation of overtones of the ν_1 mode of C–H bonds in CF_2HCl, because the main excitation mechanism at a laser light intensity of ≈ 100 TW cm^{-2} required in these experiments proved to be the field ionization. The expansion of the IR spectral range of the facility allowed us to excite selectively the fundamental vibrations of basic molecular bonds and to study the dynamics of intramolecular processes initiated by multi-

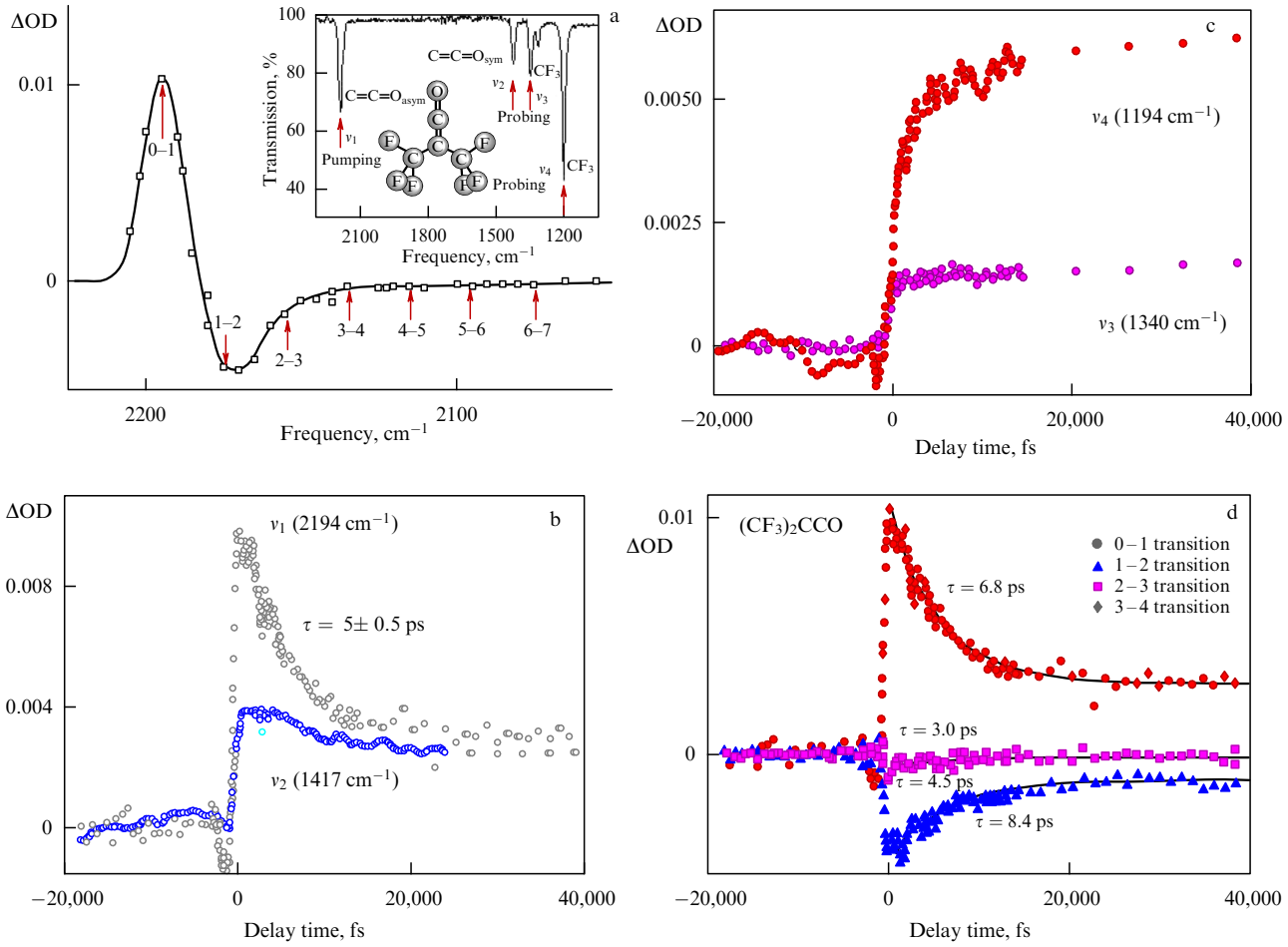

Figure 1. $(CF_3)_2CCO$ molecule: (a) difference induced absorption spectrum ΔOD for the delay τ_d = 1 ps between pump and probe pulses upon excitation and probing of different transitions of the mode ν_1 indicated in the figure (OD is abbr. of optical density); the inset shows the linear absorption spectrum. (b, c) ΔOD dynamics upon excitation of the ν_1 mode and probing at the 0 – 1 vibrational transition for different vibrational modes. (d) ΔOD dynamics at different vibrational transitions of the mode ν_1 in the $ICF_2C=OF$ molecule; solid curves fit the single-exponential approximation.

photon IR excitation. In IR pump–probe experiments [9–13] performed together with E A Ryabov's group, we investigated the vibrational dynamics in a group of molecules with the chromophore C=O bond excited by femtosecond pulses at a wavelength of 4.6–5.8 μm.

The selective multiphoton excitation of the $\nu_1 = 2194$ cm^{-1} mode in the $(CF_3)_2CCO$ molecule was observed up to the vibrational level $v = 7$ ($\approx 15{,}000$ cm^{-1}) (Fig. 1a) with the characteristic relaxation time $\tau_{IVR} = 5 \pm 0.3$ ps (Fig. 1b). The 'instant' ($\tau \ll \tau_{IVR}$) induced absorption signal ΔOD appeared in nonresonant modes ν_2, ν_3, and ν_4 as well (Fig. 1b, c), but the corresponding relaxation times and the sign of the change were different for various modes, which is related to distinct ways and types of migration of the vibrational energy.

The characteristic relaxation times τ_{IVR} at the 0 – 1 vibrational transition in iron and chromium carbonyls differ by 2 – 3 orders of magnitude from intramolecular relaxation times of other molecules studied (see Table 1). An analysis of the obtained results revealed a correlation between τ_{IVR} and the density of the four-frequency Fermi resonances in the vicinity of the first excited vibrational level [13]. The decrease in τ_{IVR} observed for ICF_2COF upon increasing the vibrational excitation level of the molecule (Fig. 1d) is also caused by the increase in the density of states.

Table 1. Characteristic intramolecular relaxation times τ_{IVR} at the 0 – 1 vibrational transition for molecules studied upon exciting vibrations of the C=0 bond.

Molecule	$\nu_{C=O}$, cm^{-1}	τ_{IVR}, ps
C_4F_9COI	1793	2.4 ± 0.3
$(CF_3)_2CO$	1804	3.5 ± 0.5
$(CF_3)_2CCO$	2194	5.0 ± 0.3
ICF_2COF	1880	6.8 ± 0.2
$H_3C-COOC_2H_5$	1756	8.0 ± 0.3
$H_2C=CH-COOC_2H_5$	1751	8 ± 1.5
		80 ± 15
$HCOOC_2H_5$	1750	20 ± 1
$Fe(CO)_5$	2014	1000 ± 300
$Cr(CO)_6$	2000	1500 ± 500

3.1.2 Formation of microstructured surface films upon irradiation of polyatomic molecules by femtosecond IR laser pulses. Experiments on gas phases revealed the formation of microstructures on the surface of BaF_2 and LiF dielectric substrates, which were produced from the decomposition of molecules irradiated by femtosecond IR laser pulses. In the case of $Fe(CO)_5$ and $Cr(CO)_6$ metal carbonils, such films began to form after the multiphoton IR dissociation of these molecules in the gas phase [12, 14, 15]. However, the

resonance action of femtosecond IR laser pulses with an intensity up to ~ 2.5 TW cm^{-2} on the vibration of the C=C=O bond in similar experiments with $(CF_3)_2CCO$ and some other molecules, including silicon-containing molecules, did not result in the decomposition of these molecules in the gas phase. Nevertheless, the growth of microstructures was observed at the radiation intensity by an order of magnitude lower, $\sim 10^{11}$ W cm^{-2} [12, 16], and not only upon the resonance action, but also upon irradiation at wavelengths ranging from 3.3 to 5.4 μm. The analysis of experimental data shows that molecules are decomposed in a physically adsorbed layer, probably due to ionization by electrons accelerated in the electric field of laser radiation in the near-surface layer of a dielectric substrate. This is consistent with a decrease in the growth efficiency of microstructures observed when increasing the ionization potential of molecules under consideration [12, 16].

3.1.3 Decomposition of molecular nanoclusters upon multiphoton excitation by femtosecond laser pulses. Reactions in clusters with the formation of I_2 and I_2^+ were observed upon excitation of alkyl iodide clusters by nanosecond UV pulses [17]. However, their rates were measured only upon excitation of $(CF_3I)_N$ by femtosecond UV pulses [18, 19]. The source of cluster beams was a pulsed supersonic nozzle. Free molecules being produced after the decomposition of clusters were ionized by a 266-nm probe pulse with a variable delay t_d and detected with a photoionization time-of-flight mass spectrometer.

It was found that the ionization of clusters by femtosecond pulses resulted in the formation of a considerably broader set of ion products with much steeper dependences of their yield on the radiation intensity than upon ionization by nanosecond pulses at the same wavelength.

The direct observation of the formation kinetics of I_2^+ molecular ions upon femtosecond ionization of $(CF_3I)_n$ clusters revealed two characteristic times corresponding to two possible reaction channels. The first, with the characteristic time $\tau_1 \approx 1$ ps, is realized directly in the initial cluster for specific 'dimer-like' configurations, in which two iodine atoms of neighboring CF_3I molecules are separated by the minimal distance. In the second channel, structures favorable for the formation of I_2^+ are produced for the time $\tau_2 \approx 7$ ps due to the structural rearrangement initiated by a pump pulse in clusters.

The same scheme was used in Ref. [20] for studying the intramolecular and intracluster dynamics by exciting *vibrational degrees of freedom* with femtosecond IR laser pulses.

3.2 Study of the femtosecond dynamics in condensed media by the pump–probe method in a broad spectral range

The photoinduced response upon excitation and probing at the same laser wavelength (the 'degenerate' scheme) does not allow one to determine unambiguously the evolution of a nonequilibrium state. In experiments performed at ISAN, a broadband probing by supercontinuum pulses or parametrically transformed pulses is applied. In addition, the equipment at ISAN CCU makes it possible to perform investigations at different excitation wavelengths, which considerably enriches the information obtained.

3.2.1 Study of the ultrafast dynamics of electrons and coherent phonons in a bismuth single crystal. The absorption of the energy of femtosecond laser pulses by electrons in matter for a time interval that is small compared to the characteristic time of motion of atoms significantly changes the interatomic potential. This leads to such effects as nonthermal melting, ultrafast structural transitions in the solid phase, and the generation of coherent phonons — the intense coherent vibrations of atoms at the phonon mode frequency. The necessary condition for excitation of coherent phonons is the presence of combination-active transitions at the corresponding frequencies and an excitation pulse with a duration smaller than the oscillation period. The detection of coherent phonons can give valuable information about ultrafast processes in condensed media, which is inaccessible for stationary spectroscopy.

Due to the large value of the deformation potential, bismuth proved to be one of the first nontransparent solids in which the A_{1g} coherent phonon modes were excited (the out-of-phase displacements of atoms along the trigonal axis) (Fig. 2). Although all previous experiments had been performed applying the 'degenerate' scheme, some interesting effects were observed at high enough excitation intensities, in particular, the 'softening' in the oscillation frequency appearing at the excitation instant of time.

We studied the photoinduced response $\Delta R/R(t)$ (the relative change in the reflection coefficient) of bismuth for the first time in the excitation and probe wavelength range from visible to near-IR [21–25]. The signal (Fig. 2a) consisted of a set of oscillations decaying at the rate γ, which were caused by a coherent phonon with the frequency ν_A, and the monotonic response $(\Delta R/R)_{mon}$ characterizing the relaxation of photoexcited charge carriers and incoherent (nonthermal) lattice processes:

$$\frac{\Delta R}{R} = A \exp(-\gamma t) \cos\left(\nu_A(t) t\right) + \left(\frac{\Delta R}{R}\right)_{mon}, \qquad (1)$$

where A is the oscillation amplitude. It turned out that $(\Delta R/R)_{mon}$ decayed at three characteristic times $\tau_1 = 1.0 \pm 0.3$ ps, $\tau_2 = 7.0 \pm 0.5$ ps, and a considerably longer time (1.5 ns, according to our measurements), which is assumed infinite for $(\Delta R/R)_{mon}$:

$$\left(\frac{\Delta R}{R}\right)_{mon} = \sigma_1 \exp\left(-\frac{t}{\tau_1}\right) + \sigma_2 \exp\left(-\frac{t}{\tau_2}\right) + \sigma_3 . \qquad (2)$$

This meant that pulsed laser excitation produces in bismuth three groups of nonequilibrium electrons with substantially different relaxation rates. Because optical probing makes possible measuring the dynamics of coherent phonons and their decay only through their electronic component having its own complicated dynamics, the data obtained were compared to the results of probing photoexcited bismuth by ultrafast X-ray pulses, allowing the direct detection of atomic positions. The similarity between characteristic relaxation times of the decay and the frequency shift of coherent oscillations measured under equivalent excitation conditions [22] prove that probing by femtosecond laser pulses in the optical range gives the same information about coherent phonons in bismuth as X-ray measurements, but with the better time resolution and sensitivity.

It was revealed that the characteristic time of relaxation of the instant frequency of the A_{1g} oscillations from 2.7 THz at the excitation moment at a wavelength of 800 nm (for the excitation energy density 1.2 mJ cm^{-2}) to the equilibrium

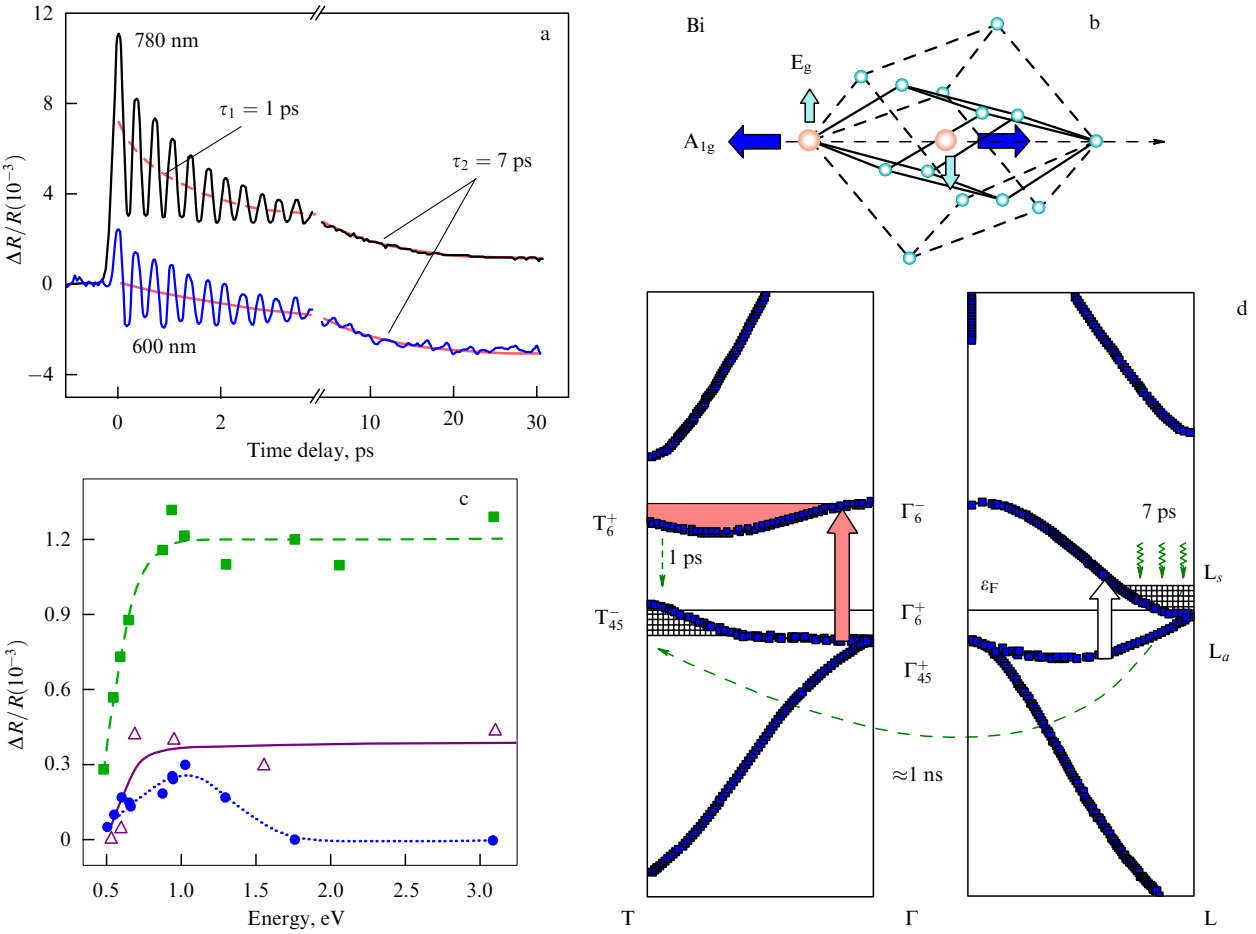

Figure 2. (a) Photoinduced response of bismuth at wavelengths 600 and 780 nm (the 1.3-mJ cm^{-2} excitation is at 400 nm). Solid and dashed curves correspond to the slow and fast components of $(\Delta R/R)_{\text{mon}}$, respectively. (b) The structure of a bismuth single crystal. The arrows indicate the direction of motion of atoms in the unit cell (shown by large spheres) during vibrations in the totally symmetric A_{1g} mode and doubly degenerate E_g mode. (c) Amplitudes of coherent phonons of A_{1g} (squares), E_g (circles) and 1-ps components of $A_{\sigma 1}$ (triangles) modes as functions of the excitation quantum energy. (d) Part of the band structure of bismuth with the identification of different electron groups. The dark heavy arrow marks the resonance excitation of electrons resulting in the appearance of the 1-ps component and generation of A_{1g} phonons. The light heavy arrow illustrates 'intraband' transitions causing only the charge accumulation near the Fermi level. The hatched regions denote excited electrons (L point) and holes (T point) with a nanosecond lifetime.

value of 2.93 THz obtained in Raman scattering experiments coincides with the characteristic relaxation time τ_1 of the fast component of monotonic response (2). This indicates a strong coupling between the A_{1g} phonon mode and a group of electrons with the 1-picosecond dynamics, because the 'frequency softening' effect is caused by the influence of excited electrons on the interatomic potential in a bismuth crystal. This assumption was confirmed in experimental studies of the relaxation dynamics of coherent phonons in bismuth excited in the spectral range from 400 to 2300 nm [24, 25], which have demonstrated the same spectral dependences of the amplitude A of the A_{1g} coherent phonons and σ_1. A considerable decrease in the generation efficiency of coherent phonons for quantum energies < 0.7 eV (Fig. 2c) is explained by excitation of nonequilibrium electrons and holes at points L and T, respectively, near the Fermi level (Fig. 2d), which are weakly coupled with the lattice. In this case, relaxation with the characteristic time ≈ 1 ns represents their indirect recombination, while the incoherent dynamics with the characteristic time ≈ 7 ps are related to crystal lattice heating.

For lower excitation energy densities (on the order of 0.1 mJ cm^{-2}), the doubly degenerate E_g phonon mode was also observed in parallel with the totally symmetric A_{1g} mode. The spectral dependence of the generation efficiency of the A_{1g} mode remained the same as in previous experiments. However, beginning from $\lambda \sim 800$ nm, the amplitude of the E_g mode starts to increase, reaching the maximum near $\lambda = 1300$ nm (≈ 1 eV) (Fig. 2c), which corresponds to the spectral dependence of the Raman scattering cross section. A comparison between the spectral dependences of the amplitude of the E_g and A_{1g} coherent phonons and Raman scattering cross sections showed that generation mechanisms for coherent phonons with different symmetries are distinct. It was found that the displacements of equilibrium positions are the main mechanism in the generation of A_{1g} coherent phonons, and this mechanism cannot be reduced to the resonant Raman scattering responsible for the coherent excitation of low-symmetry phonon modes.

3.2.2 Relaxation dynamics of optical excitations in conducting polymers. The broadband femtosecond pump–probe technique was applied to studying the features of relaxation of an initially doped semioxidized polyaniline form, emeraldine, which is, according to Ref. [26], a metal state with a half-filled conduction band. The main goal of the experiment was to understand the nature of primary excitations in this polymer

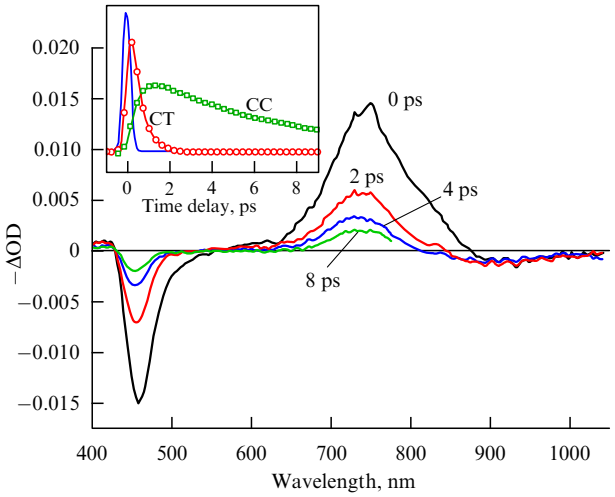

Figure 3. Difference transmission spectra of initially doped polyaniline measured for delays indicated in the figure upon excitation by femtosecond pulses at 400 and 800 nm. The inset gives the results of experimental data processing by the *Global Analysis* method. The solid curve is the correlation function of the exciting and probe pulses. The two other dependences characterize the formation and decay dynamics of charge-transfer (CT) excitons and free carriers (CC).

excited into 400- and 800-nm bands. The difference spectra exhibited three distinct features: the bleaching of the 750-nm band and photoinduced absorption with the center at 460 nm and in the wavelength range from 850 to 1050 nm [27] (Fig. 3). The processing of the experimental results (see inset to Fig. 3) revealed that the dynamics of the 750-nm band are related to excitons; the longer-wavelength part reflects the appearance of charge carriers, but the main changes in the difference spectrum are related to electric fields [28]. Near the zero delay time, this is the electric field of the exciting pulse (the Stark effect in an alternating field). For longer delays, the electric field is produced by free electric charges appearing in the dissociation of excitons with the characteristic time ≈ 1 ps and recombining for 7 ps. It was found that no more than 1% of excitons produced upon laser excitation decay into individual charged quasiparticles, while the others rapidly recombine.

As a result, it was shown that the primary photoproduct does not comprise charge carriers but neutral charge-transfer excitons, which makes the employment of the concept of a molecular crystal preferable over the band model.

3.3 Experiments with photoelectrons

3.3.1 Laser projection microscope (LPM). The idea of replacing the field emission in the Muller electron microscope, which cannot be used for studying complex polyatomic organic molecules because of the distortion of their structure up to their destruction in a strong electric field, by much more 'soft' electron (ion) emission produced by laser radiation was suggested by Letokhov [29] in 1975. This method, along with the spatial resolution, provided the spectral selectivity, because electrons (or ions) forming an image can be produced upon selective laser excitation followed by the ionization of a part of the molecule with a certain molecular bond. In this case, the radial static electric field performs in the LPM only the 'transport' function. The use of ultrashort laser pulses could also provide very high time resolution. In addition, the high intensity of ultrashort pulses at comparatively low energies makes possible laser-induced multiphoton emission with the minimal heating of samples.

Photoion images with a magnification of $\approx 10^3$ upon selective excitation of dye molecules by ultrashort pulses were obtained in Refs [30, 31]. However, a rather low spatial resolution determined by the scatter in the kinetic energy of molecular photoions desorbed from the surface (at a level of 10 eV) and the destructive nature of the study severely restrict the potential of this method. As a result, the photoelectron regime of the LPM proved to be preferable.

In 2004, it was proposed that a quartz nanocapillary be utilized instead of a classic needle. After the deposition of a conducting layer on such a capillary, an electrostatic potential can be applied to it for investigating samples by the method of photoelectron nanoaperture LPM [32, 33]. In addition, spatially compressed electron and ion bunches were prepared by passing them through nanocapillaries [34–36], and X-rays were concentrated [37]. This permits the construction of nano-sized electron, ion or soft X-ray sources that can be precisely moved along a surface with the aid of a vacuum piezoelectric translator (scanning vacuum microscopy) [38].

The irradiation of a photoelectron beam by intense tightly focused ultrashort laser pulses leads to the pulsed scattering of electrons flying in a light field under the action of the Gaponov–Miller force [39]. This, together with the employment of the projection principle, permits one to combine the spatial and time resolutions in one experiment [40].

3.3.2 Projection nanoaperture microscopy of a conducting polyaniline polymer. It is known that redox-heterogeneous structures (regions with different oxidation degrees contacting with each other) strongly affect the electric conduction of polyaniline (PANI), the most promising representative of conducting polymers (see Section 3.2.2). The redox-heterogeneity of semioxidized PANI on a macroscopic level was found with the help of Kelvin microscopy [41]. In experiments with the nanoaperture LPM, the PANI structure was visualized and its redox-heterogeneity at the nanometer scale was discovered, which is of great theoretical and practical interest [42].

A commercial 100-nm quartz capillary covered with a polymer layer was utilized as a needle in the microscope, to which the electric potential $U = -3500$ V was applied (Fig. 4a). An oilless vacuum in a chamber was maintained at a level of 10^{-7} mmHg. The capillary end was irradiated by 400-nm and 800-nm laser pulses shorter than 100 fs. The photoemission image of the capillary aperture (Fig. 4c) recorded with a position-sensitive detector gives the spatial magnification of the microscope as $\approx 2 \times 10^5$.

The PANI images obtained upon irradiation at wavelengths of 400 and 800 nm are presented in Fig. 4d, e, respectively. Light and dark regions correspond to the high and low densities of the photoemission signal, respectively. The PANI film under study predominantly consists of the reduced form with the absorption maximum at ~ 350 nm and the semioxidized form efficiently absorbing radiation at 400 and 800 nm (Fig. 4d, e) [43]. Consequently, upon irradiation at $\lambda_1 = 400$ nm, photoemission centers in the image obtained should be more densely packed than upon irradiation at $\lambda_2 \approx 800$ nm, as observed in experiments (Fig. 4d, e). This confirms in experiment the existence of

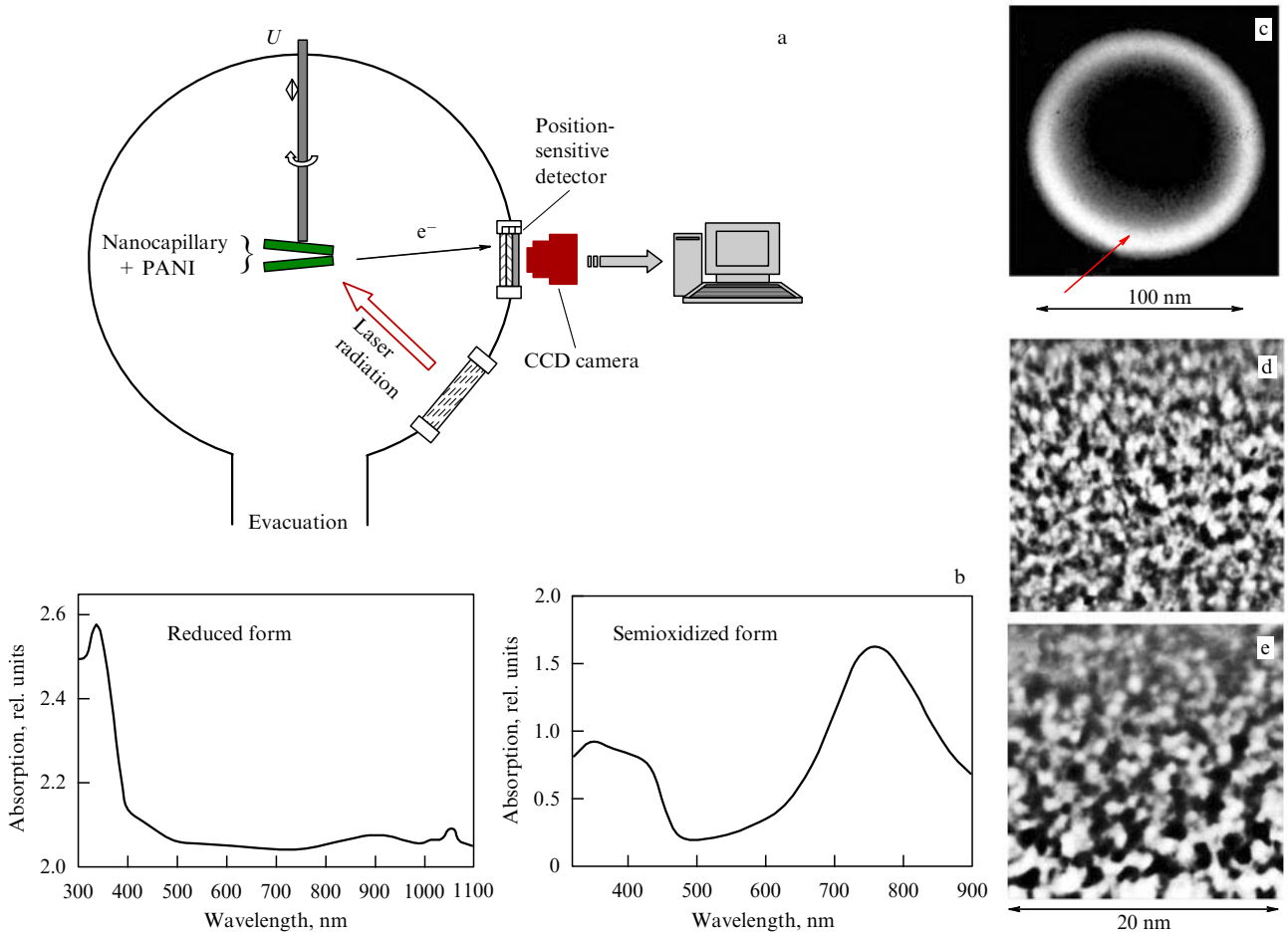

Figure 4. (a) Schematic of the experiment on determining the nanoscale of PANI redox-heterogeneity with a projection nanoaperture microscope. (b) Characteristic absorption spectra of the reduced and semioxidized PANI forms. (c) Photoemission image of the capillary aperture. (d, e) Enlarged parts of the image presented in figure (c) upon irradiation at 400 and 800 nm, respectively.

the PANI redox-heterogeneity in wavelength ranges from nanometers to a macroscopic scale.

4. Studies expanding the possibilities of the laser complex

4.1 Nanolocal desorption of complicated molecular complexes with the help of a compact pulsed X-ray source based on a femtosecond laser

At present, the desorption effected by soft X-rays is studied only with the aid of synchrotrons. The authors of Refs [44, 45] demonstrated for the first time the desorption of complicated molecular complexes by soft X-ray pulses produced upon irradiation of a metal target by 10^{16}-W cm^{-2} femtosecond laser pulses and collimated in a 100-nm quartz capillary (Fig. 5). The presence of heavy masses in time-of-flight mass spectra of a conducting organic polymer PANI upon X-ray desorption demonstrates the difference between this 'soft' regime and the 'plasma' character of photodesorption by intense laser radiation in the visible region, resulting in a stronger fragmentation of polyaniline (see Fig. 5). These results open up the possibility of studying surfaces with spatial nanoresolution in conjunction with the high elemental (chemical) selectivity, and also of observing the photodesorption process with a high time resolution.

4.2 Expansion of the spectral range of the laser facility to the terahertz region

The change in the spectrum of a femtosecond laser pulse with an inclined front due to the efficient generation of terahertz radiation in $LiNbO_3$ by the method of optical rectification was found in Ref. [46]. Ultrashort terahertz pulses were generated with an energy conversion efficiency up to 0.25%, corresponding to a 250% conversion of the number of photons [47].

4.3 Temporary profile conversion of ultrashort pulses in a one-dimensional photonic crystal

Diffraction-induced pulse splitting was found experimentally under conditions of dynamic Bragg diffraction in the Laue geometry in linear one-dimensional photonic crystals into two [48] and more [49] pulses due to the difference in the group velocities of modes propagating in regions with various refractive indices. Changing the parameters of a photonic crystal and the input pulse makes possible controlling the temporal structure of the output train of pulses and compressing selectively or focusing one of the pulses in parallel with the simultaneous broadening or defocusing of another pulse.

4.4 Light bullets

Upon filamentation of a 70-fs pulse in a 2-cm-thick silica sample in the anomalous dispersion region (1800 nm) [50], IR

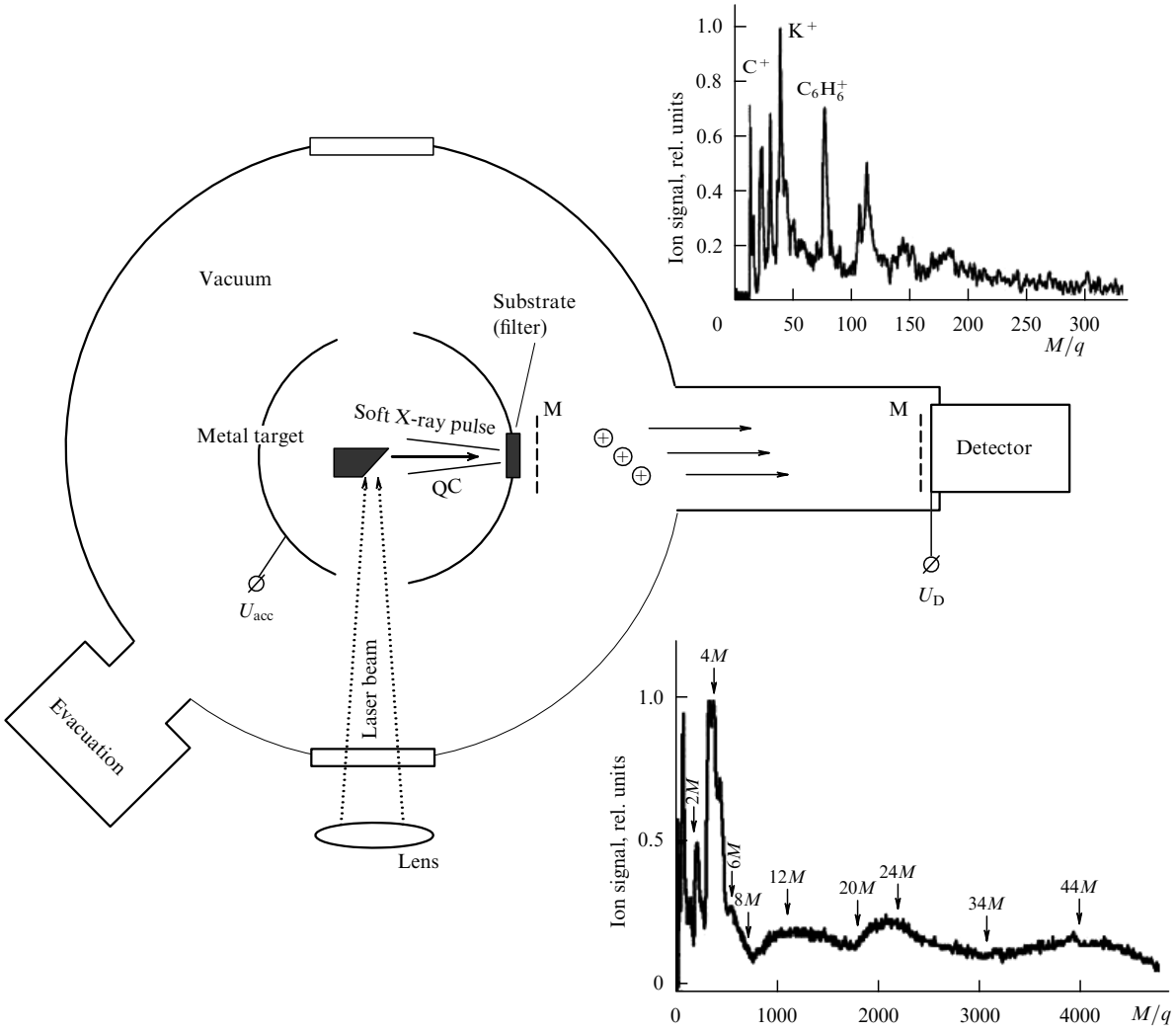

Figure 5. Schematics of the experiment. Organic polymer PANI is deposited on a 3-μm-thick Mylar substrate with a 120-nm-thick gold cover playing the part of a filter for soft X-rays (200–250 eV): QC is a quartz capillary with a 100-nm output aperture, M are grounded metal grids, U_{acc} is the accelerating voltage, U_d is the voltage across a detector. The mass spectrum at the top of the figure is obtained upon desorption by an 800-nm pulse (heavy masses are absent); M/q is the ratio of the ion mass (in atomic mass units) to its charge multiplicity. The mass spectrum at the bottom of the figure is obtained upon desorption by a soft X-ray pulse; here, M is the mass of the molecular PANI ion (scales along horizontal axes are substantially different).

light bullets with high spatio-temporal energy localization were produced and detected by the autocorrelation method [51, 52]. The minimum duration of a 2.7-μJ light bullet separated at the output from the sample from the near-axial part of the filament by a 50-μm aperture did not exceed 11 fs, i.e., approximately two optical periods. The results of numerical simulations for specified experimental parameters are consistent with experimental data.

5. Conclusion

The unique combination of the capacities of the Optical Spectral Studies femtosecond laser facility at ISAN CCU are far from being restricted to the applications considered above. Active work is also underway on the dynamics of excitons and charge carriers in new biologically compatible composite materials based on nanocrystalline silicon, the nonlinear response of quantum wells in semiconductors, and the nonlinear properties of electron gas in crystalline and nanostructured semimetals. By using the pump–probe technique in the terahertz region, the study of the relaxation of low-energy electron excitations in new low-dimensional systems with the Dirac linear dispersion law has been initiated. The first 4D microscope in Russia was developed and is being operated, which combines a transmission electron microscope with a modern pulsed laser setup producing ultrashort electron beams. The 4D microscope will be applied for studying fast processes initiated by ultrashort laser pulses in promising new materials and structures with a high spatio-temporal resolution.

Acknowledgments

The author is deeply grateful to E A Ryabov, S A Aseev, A A Mel'nikov, V O Kompanets, V P Kandidov, V B Laptev, V N Lokhman, B N Mironov, Yu E Lozovik, V O Misochko, A A Makarov, B I Mantsizov, S V Pigul'skii, D G Poidashev, S E Svyakhovskiy, E O Smetanina, V F Ivanov, and A P Cherkun for their collaboration and many stimulating discussions.

This work was supported by the Russian Foundation for Basic Research (grants Nos 13-02-00927, 13-02-00260, and 14-02-00558).

References

1. Chekalin S V *JETP* **103** 756 (2006); *Zh. Eksp. Teor. Fiz.* **130** 873 (2006)
2. Chekalin S V *Phys. Usp.* **49** 634 (2006); *Usp. Fiz. Nauk* **176** 657 (2006)
3. Letokhov V S et al. *Lazernaya Pikosekundnaya Spektroskopiya i Fotokhimiya Biomolekul* (Laser Picosecond Spectroscopy and Photochemistry of Biomolecules) (Moscow: Nauka, 1987); Zherikhin A N, Ph.D. Thesis, Phys. Math. Sciences (Troitsk: Institute of Spectroscopy, Acad. Sci. USSR, 1981); Sharkov A V, Ph.D. Thesis, Phys. Math. Sciences (Troitsk: Institute of Spectroscopy, Acad. Sci. USSR, 1981)
4. Zherikhin A N et al. *Sov. J. Quantum Electron.* **4** 525 (1974); *Kvantovaya Elektron.* **1** 956 (1974)
5. Kryukov P G *Quantum Electron.* **31** 95 (2001); *Kvantovaya Elektron.* **31** 95 (2001)
6. Matveets Yu A, Semchishen V A *Sov. J. Quantum Electron.* **9** 503 (1979); *Kvantovaya Elektron.* **6** 848 (1979)
7. Sharkov A V et al. *Photochem. Photobiol.* **38** 109 (1983); Matveetz Yu A, Chekalin S V, Sharkov A V *J. Opt. Soc. Am. B* **2** 634 (1985); Sharkov A V et al. *Biochim. Biophys. Acta BBA Bioenerg.* **808** 94 (1985); *Dokl. Akad. Nauk SSSR* **281** 466 (1985)
8. Apatin V M et al. *JETP Lett.* **80** 95 (2004); *Pis'ma Zh. Eksp. Teor. Fiz.* **80** 104 (2004); *Chem. Phys. Lett.* **414** 76 (2005)
9. Kompanets V O et al. *JETP Lett.* **92** 135 (2010); *Pis'ma Zh. Eksp. Teor. Fiz.* **92** 157 (2010)
10. Kompanets V O et al. *Bull. Russ. Acad. Sci. Phys.* **75** 145 (2011); *Izv. Ross. Akad. Nauk Ser. Fiz.* **75** 160 (2011)
11. Chekalin S V et al. *Chem. Phys. Lett.* **512** 178 (2011)
12. Kompanets V O et al. *Quantum Electron.* **43** 320 (2013); *Kvantovaya Elektron.* **43** 320 (2013)
13. Chekalin S V et al. *J. Phys. Chem. A* **118** 955 (2014)
14. Kompanets V O et al. *Tech. Phys. Lett.* **35** 720 (2009); *Pis'ma Zh. Tekh. Fiz.* **35** (15) 71 (2009)
15. Kompanets V O et al. *Perspek. Mater.* (8) 141 (2010) Special issue
16. Kompanets V O et al. *Laser Phys.* **23** 056004 (2013)
17. Taatjes C A et al. *J. Chem. Phys.* **98** 4355 (1993)
18. Apatin V M et al. *JETP Lett.* **94** 570 (2011); *Pis'ma Zh. Eksp. Teor. Fiz.* **94** 610 (2011)
19. Apatin V M et al. *JETP* **115** 567 (2012); *Zh. Eksp. Teor. Fiz.* **142** 644 (2012)
20. Chekalin S V et al., in *The Intern. Conf. on Coherent and Nonlinear Optics, ICONO/LAT 2013, June 18–22, 2013, Moscow, Russia*, Conference Program (Moscow, 2013) p. 41, ITuK5
21. Melnikov A A et al. *JETP* **111** 431 (2010); *Zh. Eksp. Teor. Fiz.* **138** 486 (2010)
22. Mel'nikov A A, Misochko O V, Chekalin S V *JETP Lett.* **89** 129 (2009); *Pis'ma Zh. Eksp. Teor. Fiz.* **89** 148 (2009)
23. Melnikov A A, Misochko O V, Chekalin S V *Phys. Lett. A* **375** 2017 (2011)
24. Mel'nikov A A, Misochko O V, Chekalin S V *Quantum Electron.* **43** 313 (2013); *Kvantovaya Elektron.* **43** 313 (2013)
25. Melnikov A A, Misochko O V, Chekalin S V *J. Appl. Phys.* **114** 033502 (2013)
26. MacDiarmid A G *Synth. Met.* **125** 11 (2001)
27. Melnikov A A, Chekalin S V *J. Phys. Chem. B* **113** 13454 (2009)
28. Melnikov A, Ivanov V, Chekalin S *Chem. Phys. Lett.* **488** 38 (2010)
29. Letokhov V S *Phys. Lett. A* **51** 231 (1975)
30. Letokhov V S et al. *Sov. J. Quantum Electron.* **12** 1377 (1982); *Kvantovaya Elektron.* **9** 2117 (1982)
31. Chekalin S V et al. *Appl. Phys. B* **33** 57 (1984)
32. Aseev S A et al. *JETP Lett.* **80** 568 (2004); *Pis'ma Zh. Eksp. Teor. Fiz.* **80** 645 (2004)
33. Mironov B N et al. *JETP* **101** 628 (2005); *Zh. Eksp. Teor. Fiz.* **128** 732 (2005)
34. Aseyev S A et al. *Appl. Phys. Lett.* **89** 112513 (2006)
35. Aseev S A et al. *Bull. Russ. Acad. Sci. Phys.* **74** 931 (2010); *Izv. Ross. Akad. Nauk Ser. Fiz.* **74** 972 (2010)
36. Aseev S A et al. *JETP Lett.* **87** 361 (2008); *Pis'ma Zh. Eksp. Teor. Fiz.* **87** 422 (2008)
37. Mironov B N, Aseev S A, Chekalin S V, in *7-ya Mezhdunarodnaya Nauchnaya Konf. "Lazernaya Fizika i Opticheskie Tekhnologii". Sbornik Nauchnykh Trudov Konf.* (7th Intern. Scientific Conf. on Laser Physics and Optical Technologies. Collection of Scientific Works of the Conf.) Vol. 2 (Minsk, 2008) p. 125
38. Aseyev S A et al. *Quantum Electron.* **43** 308 (2013); *Kvantovaya Elektron.* **43** 308 (2013)
39. Aseyev S A et al. *JETP* **112** 780 (2011); *Zh. Eksp. Teor. Fiz.* **139** 894 (2011)
40. Aseev S A et al. *JETP Lett.* **90** 13 (2009); *Pis'ma Zh. Eksp. Teor. Fiz.* **90** 15 (2009)
41. Ivanov V F et al. *Synth. Met.* **152** 153 (2005)
42. Mironov B N et al. *JETP Lett.* **92** 779 (2011); *Pis'ma Zh. Eksp. Teor. Fiz.* **92** 859 (2010)
43. Ivanov V F et al. *Proc. Mater. Res. Soc.* **600** 221 (2000)
44. Mironov B N et al. *JETP Lett.* **96** 601 (2012); *Pis'ma Zh. Eksp. Teor. Fiz.* **96** 670 (2012)
45. Aseyev S A, Mironov B N, Chekalin S V *J. Chem. Phys.* **139** 144202 (2013)
46. Stepanov A G et al. *JETP Lett.* **85** 227 (2007); *Pis'ma Zh. Eksp. Teor. Fiz.* **85** 279 (2007)
47. Stepanov A G et al. *Opt. Lett.* **33** 2497 (2008)
48. Svyakhovskiy S E et al. *Phys. Rev. A* **86** 013843 (2012)
49. Svyakhovskiy S E et al. *J. Opt. Soc. Am. B* **30** 1261 (2013)
50. Chekalin S V, Kandidov V P *Phys. Usp.* **56** 123 (2013); *Usp. Fiz. Nauk* **183** 133 (2013)
51. Chekalin S V et al. *Quantum Electron.* **43** 326 (2013); *Kvantovaya Elektron.* **43** 326 (2013)
52. Smetanina E O et al. *Laser Phys. Lett.* **10** 105401 (2013)